第 29 卷 第 6 期
2008 年 6 月

焊 接 学 报
TRANSACTIONS OF THE CHINA WELDING INSTITUTION

Vol. 29 No. 6
June 2008

基于结构光的水下焊接熔池宽度在线检测

张为民[1,2]， 王国荣[1]， 石永华[1]， 李鹤喜[1]
(1. 华南理工大学 机械工程学院, 广州 510640;
2. 广州航海高等专科学校 计算机与信息工程系, 广州 510725)

张为民

摘 要：直接拍摄水下焊接熔池图像来检测焊接熔池宽度实现难度较大，提出了一种通过成形焊缝结构光条纹图像来完成水下焊接熔池宽度在线检测的方法。将装有防水罩的激光结构光视觉传感器安装在焊枪之后置于水下，针对水下成形焊缝图像特点，经图像加窗、拉普拉斯锐化、二值化以及数学形态学滤波和图像细化处理，就能够在线获得焊接熔池宽度。结果表明，处理过程速度快，检测结果精度高。当条纹检测点和熔池中心之间的距离小于 35 mm 时，焊接熔池宽度相对误差可控制在 3% 以内。

关键词：水下焊接；焊接熔池宽度；条纹结构光；图像处理
中图分类号：TG409 文献标识码：A 文章编号：0253-360X(2008)06-0033-04

0 序 言

水下焊接是船舶、船坞、港口设施、海洋油气、海底管道等设施建造和维修必不可少的关键技术和工艺之一。水下焊接时，特别是水下湿法焊接时电弧周围产生大量气泡和烟雾，焊接熔池区域可见度非常低，潜水焊工基本属于盲焊，非常容易出现焊接缺陷。利用弧光或普通光源和摄像机组成的视觉系统虽然成本低、结构简单，但水体及溶于水体的有机物质和悬浮颗粒会吸收光能量，还会产生散射影响。不但减少了光能量，而且产生的散射光还会形成大量背景光噪声，降低成像信噪比和对比度[1]。再加上强烈的弧光干扰以及大量的气泡和烟雾等的影响，直接拍摄水下焊接熔池很难获得较清晰的图像。华南理工大学水下焊接实验室利用各种各样的滤光系统直接拍摄水下焊接熔池图像，效果都不太理想。与普通光源或弧光相比激光结构光具有单色性好、方向性好、亮度高、干涉性好、能量密度集中等优点。特别是单条纹结构光可以在工件上形成一条很窄的光带，通过 CCD 产生的变形能准确反映成形焊缝形状。当满足一定的检测条件，工程实际中成形焊缝宽度就可以代表焊接熔池宽度[2]。作者应用单条纹激光结构光视觉系统实现了水下焊接熔池宽度的在线检测，同时还总结了条纹检测点和熔池中心之间的距离与焊接熔池宽度相对误差的关系。

1 结构光图像检测原理及系统构成

采用的水下激光结构光视觉传感器主要由 CCD 摄像机、滤光片、激光二极管和透镜等部分组成[3]。工作时，将带有防水罩的激光结构光视觉传感器安装在焊枪之后置于水下。激光二极管发出的光经透镜后变成一条结构光照射到工件上，形成一条很窄的光带。摄像机和激光光源以 20°～90°的角度(一般是45°)固定于焊接件表面对称面上，激光束横向投射到成形焊缝上，CCD 摄像机接收条形激光图像。当光带投射到成形焊缝上时，各点的深度不同。通过针孔成像后，反射到 CCD 上的位置不同。CCD 摄取图像后，再由计算机检测出反映成形焊缝形状的结构光畸变点，就可以求出成形焊缝宽度。同时，也获得了实际焊接过程焊接熔池宽度。

图 1 为实际水下焊接熔池宽度检测装置。水下

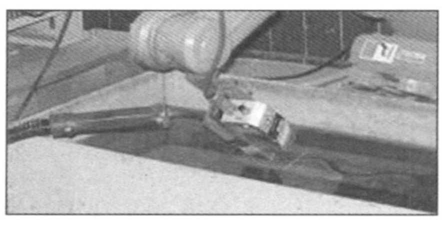

图 1 水下焊接熔池宽度检测装置
Fig 1 Underwater weld pool width detection equipment

收稿日期：2007-08-16
基金项目：国家自然科学基金资助项目(50175027)

焊接过程中水面波动较大，其折射作用会严重影响成像质量，必须在水下完成图像的拍摄。焊接时将防水罩内的激光结构光视觉传感器安装在焊枪之后置于水下。其中，防水罩由不锈钢薄板制成，在底部有一块透光度较好的玻璃。图像信号经视觉传感控制单元送入计算机机内的多通道图像采集卡，最后通过图像处理软件实现焊接熔池宽度在线检测。

2 成形焊缝图像处理

水下拍摄图像时玻璃镜面会反射发射激光束和激光二极管光源，大量的气泡和烟雾，再加上飞溅、水流以及激光散射，都会增加噪声，降低图像信噪比。如何排除各种干扰及噪声，快速、准确地获得水下焊接成形焊缝宽度，是重点要解决的问题。最终确定的成形焊缝图像处理步骤如图 2 所示。

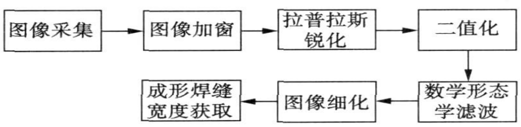

图 2 成形焊缝图像处理步骤

Fig 2 Procedure of weld image processing

2.1 图像加窗处理

图 3a 为图像采集卡采集的水下成形焊缝图像，图像大小为 256×192 像素，灰度等级为 8 位。可以看到除了成形焊缝单条纹结构光外，还有发射激光的单条纹结构光反射光纹、2 个激光二极管反射光点(因激光结构光视觉传感器有 2 个激光发射源)以及弧光、飞溅、散射和防水罩反射引起的各种噪音。结构光视觉传感器 CCD 与防水罩玻璃之间的高度固定，所以单条纹结构光反射光纹和 2 个激光二极管反射光点在图像中的位置也是固定的。而且，成形焊缝单条纹结构光是一个窄带。因此，从单条纹结构光反射光纹左侧进行图像加窗[4]，取出 60×192 的像素就可以完全包含成形焊缝单条纹结构光。加窗处理结果如图 3b 所示。不但去除了无用信息，增加了抗干扰能力。而且，待处理图像像素点减少，图像处理速度可以得到大大提高。

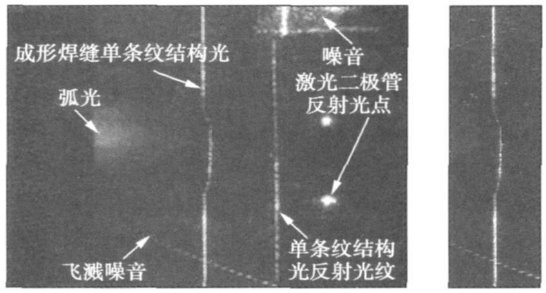

(a) 水下成形焊缝图像 (b) 加窗处理

图 3 水下成形焊缝图像加窗处理

Fig 3 Window processing of underwater weld image

2.2 拉普拉斯锐化

图像锐化可使模糊的图像变得更加清晰，从逻辑角度出发锐化处理可以用空间微分来实现。用拉普拉斯锐化算子进行图像的锐化增强[5]。一个二元图像函数的拉普拉斯变换定义为

$$\nabla^2 f=\frac{\partial^2 f}{\partial x^2}+\frac{\partial^2 f}{\partial y^2} \tag{1}$$

对于数字图像二阶偏导数定义为

$$\left.\begin{aligned}\frac{\partial^2 f}{\partial x^2}&=f(x+1,y)+f(x-1,y)-2f(x,y)\\ \frac{\partial^2 f}{\partial y^2}&=f(x,y+1)+f(x,y-1)-2f(x,y)\end{aligned}\right\} \tag{2}$$

设 $g(x,y)$ 为锐化后的图像，则

$$g(x,y)=f(x,y)-k\tau\nabla^2 f(x,y) \tag{3}$$

式中：$k\tau$ 为锐化系数，太大则会使图像中的轮廓边缘过冲，太小则锐化不明显。选 1 为锐化系数，则

$$g(x,y)=5f(x,y)-f(x+1,y)-f(x-1,y)-f(x,y+1)-f(x,y-1) \tag{4}$$

该式转换为模板运算，则为

$$\begin{bmatrix}0&-1&0\\-1&5&-1\\0&-1&0\end{bmatrix}$$

通过该模板的一次扫描可实现拉普拉斯锐化，图 4a 为经拉普拉斯锐化后的图像。

2.3 二值化

灰度图像中包含了处理对象和对象背景，如果对象灰度值大于背景灰度值，则可以采用阈值分割法对图像进行二值化[6]。即

$$f(x)=\begin{cases}0, & x\leqslant T\\255, & x>T\end{cases} \tag{5}$$

式中：T 为灰度阈值，灰度值小于等于 T 时为黑(背景)，否则为白(对象)。由图像像素灰度直方图分析得知，平均像素灰度为 20.267，背景像素灰度值集中在 10～50 之间。因此，取 $T=50$。图 4b 为锐化图像的二值化图像，可以看出噪音也加强了。

2.4 数学形态学滤波

将图形表面不断扩散以达到去除小孔的效果，称为膨胀。如用 A 表示图像集合，B 表示结构元

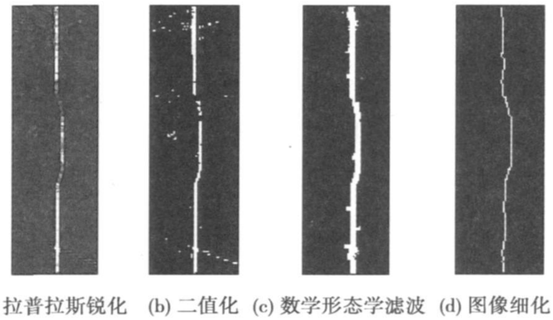

图 4　成形焊缝图像处理结果

Fig 4　Result of weld image processing

素，膨胀运算符为"$\oplus$"。反复去除图形表面像素，以达到去除点状图形的效果，称为腐蚀，腐蚀运算符为"$\ominus$"。膨胀后再腐蚀，或腐蚀后再膨胀，会产生形态变换。腐蚀后再膨胀在形态学中称为开启运算，运算符为"。"，记作 $A\circ B=(A\ominus B)\oplus B$；膨胀后再腐蚀形态学中称为闭合运算，运算符为"$\circ$"，记作 $A\circ B=(A\oplus B)\ominus B$。

膨胀处理最重要的是可以连通成形焊缝图像条纹带中的小间隙。取当前像素与它的 4 个邻点组成全方位结构元素[0 1 0；1 0 1；0 1 0] 对原二值图进行膨胀处理。拖动结构元素在待处理的图像域内移动，平移到原图像的某一点(x, y)，结构元素的像素与目标物体至少有一个像素相交，那么就保留该像素点，从而达到使物体边界向外扩张的效果[6]。利用闭运算具有填充物体内细小空洞、连接邻近物体、平滑边界、弥合小裂缝，而且本身总的位置、形状和面积不变等特性，对图像进行了全方位形态闭合运算(即 $A\circ B$)，先进行膨胀而后进行腐蚀。进一步采用小面积消除方法来消除图像中的噪声。首先对二值图像区域标记，然后对每个区域内的像素点进行统计。当二值图像的某区域面积(像素点数)在阈值以下时将该区域灰度值全部设置为零。通过对不同的成形焊缝图片统计的结果分析得出离散噪声点的像素点数一般在 10～40 之间，而闭合焊缝条纹图像像素点数至少在 250 以上。所以，设定阈值为 200，将像素点个数在 200 以下的区域全部设置为背景。处理后的图像如图 4c 所示。

2.5　图像细化

为了提取成形焊缝宽度需要找出焊缝图像中央宽度为一个像素的中心线，数学形态学可以在细化图像的同时保持图像原有形状和连通性。具体算法是针对图形边缘上的点，观察其相邻点状况，在不破坏连接性前提下，消除位于边缘的点。表达式为 $S=X-X\uparrow B$，其中 S 为图像细化后的像素集合，X 为原图像，$\uparrow$为击中击不中变换，B 为进行细化运算的结构。图 4d 为经细化处理后的图像。

2.6　成形焊缝宽度获取

细化图像由两直线段和中间的一曲线段组成，求出曲线与直线的两个交点并计算两相交点之间的距离，就可以获取成形焊缝的宽度。处理过程如下：(1) 横向逐行扫描，求出所有白点的坐标(x, y)；(2) 确定所有白点中 x 轴的坐标最小值 x_{min}；(3) 确定 x 轴坐标为 x_{min} 的所有点 y 轴坐标，找出最大值 y_{max} 和最小值 y_{min}；(4) 每像素对应的实际距离×($y_{max}-y_{min}$)，即为成形焊缝宽度。

3　试验结果

水下焊接熔池宽度在线检测试验时，焊接试样置于 100 mm 左右水深处的水平位置，由焊接机器人完成焊接过程，焊接速度为 5～7 mm/s。选用 SQJ501 气体保护药芯焊丝，直径为 ϕ1.6 mm，送丝平均速度约为 210 mm/s，焊丝伸长度为 20～25 mm。焊接电流最大值为 220～260 A，电弧电压为 25～30 V。

水下焊接试验中条纹检测点和熔池中心之间的距离在 25～40 mm 之间，记录某一时刻计算的成形焊缝宽度与焊后实测熔池宽度进行比较。采用 CPU 主频为 2.4 GHz 的计算机，图像采集周期为 40 ms，整个图像处理时间不超过 70 ms。

设条纹检测点和熔池中心之间的距离为检测距离 d，成形焊缝图像检测宽度为焊缝宽度 W，焊后实测熔池宽度为 w，绝对误差为 ΔW，相对误差为 ΔE，则

$$\Delta E=\frac{\Delta W}{w}=\frac{|W-w|}{w} \tag{6}$$

表 1 为在不同检测距离条件下，各取 4 组成形焊缝宽度与焊后实测熔池宽度作对比。其中，第 I 组平均相对误差为 3.77%；第 II 组平均相对误差为 2.79%；第 III 组平均相对误差为 2.52%；第 IV 组平均相对误差为 2.24%。则检测距离越小，平均相对误差也越小。

图 5 为在不同检测距离条件下各取 15 组采样点绘制相对误差曲线。从图中可以看出 60 组采样点焊接熔池宽度相对误差在 1.92%～4.27%之间，最大相对误差为 4.27%，平均相对误差为 2.76%。在相同检测距离条件下，相对误差随机变化。随着检测距离减小，相对误差曲线呈下降趋势。条件 I 到条件 II 相对误差下降较大。当检测距离小于 35 mm 后下降趋势较为平缓，相对误差可以控制在 3% 以内。

表1 成形焊缝宽度与熔池宽度对照表

Table 1 Comparison of weld width and weld pool width

样本序号	检测距离 d/mm	焊缝宽度 W/mm	实测宽度 w/mm	绝对误差 ΔW/mm	相对误差 ΔE(%)
Ⅰ-1	40.00	12.00	11.56	0.44	3.81
Ⅰ-2	40.00	10.16	10.54	0.38	3.61
Ⅰ-3	40.00	10.06	10.44	0.38	3.64
Ⅰ-4	40.00	10.04	10.46	0.42	4.02
Ⅱ-1	35.00	11.23	11.56	0.33	2.85
Ⅱ-2	35.00	11.45	11.16	0.29	2.60
Ⅱ-3	35.00	10.65	10.34	0.31	3.00
Ⅱ-4	35.00	10.58	10.30	0.28	2.72
Ⅲ-1	30.00	12.17	11.86	0.31	2.61
Ⅲ-2	30.00	12.14	11.86	0.28	2.36
Ⅲ-3	30.00	11.46	11.76	0.30	2.55
Ⅲ-4	30.00	11.57	11.28	0.29	2.57
Ⅳ-1	25.00	12.07	11.80	0.27	2.29
Ⅳ-2	25.00	11.89	11.64	0.25	2.15
Ⅳ-3	25.00	11.02	11.28	0.26	2.30
Ⅳ-4	25.00	10.13	10.36	0.23	2.22

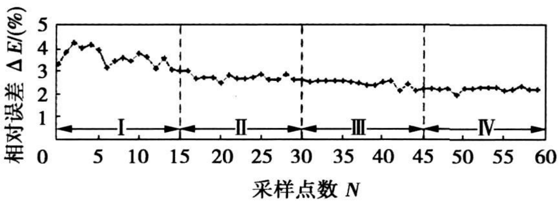

平均相对误差 2.76% 最大相对误差 4.27%

图5 焊接熔池宽度相对误差曲线

Fig. 5 Comparative error curve of weld pool width

分析在线检测误差产生的原因主要有测量过程、检测条件和图像处理等几方面。测量过程因为锈斑、飞溅噪声以及其它不稳定因素都会影响测量精度。焊前应尽量去除工件上的铁锈。而条纹检测点和熔池中心之间的距离越小，在线检测实时性越好。同时，也减小了飞溅的影响，相对误差也减小。可能的情况下应尽量减小条纹检测点和熔池中心之间的距离，最好小于35 mm。最后，图像处理中滤波效果也会影响在线检测误差。所以，应尽可能减小激光结构光视觉传感器和焊接工件之间的距离，以增强结构光亮度和对比度，获得好的图像处理效果。

4 结 论

在直接拍摄水下焊接区域获得熔池尺寸较难实现的情况下，基于条纹激光结构光视觉系统在线采集成形焊缝图像，并完成图像处理就能够在线检测水下焊接熔池宽度。条纹检测点和熔池中心之间的距离越小，焊接熔池宽度相对误差也越小。该在线检测方法实时性好，全部处理时间不超过70 ms；精度高，当条纹检测点和熔池中心之间的距离小于35 mm，焊接熔池宽度相对误差可以控制在3%以内。是一种理想的水下焊接熔池宽度在线检测方法。

参考文献：

[1] Schechner Y Y, Karpel N. Clear underwater vision[J]. Proc. Computer Vision & Pattern Recognition, 2004, 2(1): 536-543.

[2] 王其隆. 弧焊过程质量实时传感与控制[M]. 北京：机械工业出版社，2001.

[3] 孙立新，戴士杰，李 慨，等. 基于线结构光多道焊跟踪系统图像处理[J]. 焊接学报，2002，23(3)：53-55.

[4] 孙中皋，梁德群，王新年，等. 基于结构光的螺旋管焊缝自动跟踪系统[J]. 大连海事大学学报，2006，32(1)：58-61.

[5] Rahim S H, Bovik A C. Image information and visual quality[J]. IEEE Transactions Image Processing, 2006, 15(2): 430-440.

[6] 舒新宇，王国荣，刘苏宜. 一种基于数学形态学的焊缝图像处理方法[J]. 电焊机，2006，36(3)：48-51.

作者简介：张为民，男，1967年出生，讲师，博士研究生。主要研究方向为水下焊接过程监测与控制。发表论文3篇。

Email：super208956@163.com

The advantages of integrating laser power into MIG welding represent primarily increasing welding speed of hybrid welding.

Key words: hybrid welding; aluminum alloy; laser welding; arc welding

Residual stress in electric arc sprayed coatings for remanufacturing CHENG Jiangbo[1,2], LIANG Xiubing[2], CHEN Yongxiong[2], LIU Yan[2], XU Binshi[2], WU Yixiong[1] (1. Schools of Material Science and Engineering, Shanghai Jiaotong University, Shanghai 200240, China; 2. National Key Laboratory for Remanufacturing, the Academy of Armored Forces Engineering, Beijing 100072, China). p17—20

Abstract: The residual stresses in different thickness and different annealing temperatures of electric arc sprayed 7Cr13 coatings were investigated. The microstructure, elastic modulus and residual stress of the coatings were characterized by SEM, XRD, nano-indentation tester and XRD residual stress tester. The results show that the residual stress in the coating is increasing with increasing of the coating thickness. Annealing treatment can release the residual tensile stress of the coatings. When the annealing temperature is between 200—300 ℃, tensile stress can change from tenstle stress to compress stress in the coatings. The elastic modulus of the coatings is increasing with increasing of annealing temperature. Based on the results mentioned above, some advice and methods to spray forming thickness coatings can be given.

Key words: residual stress; young' s modulus; annealing; coating

Fusion-brazing joining between 5A02 aluminium alloy and Q235 steel by Nd∶YAG laser-pulsed MIG hybrid welding LEI Zhen, YU Ning, YOU Aiqing, LIN Shangyang (Harbin Welding Institute, China Academy of Machinery Sciene Technology, Harbin 150080, China). p21—24, 28

Abstract: A special type brazing flux was successfully developed. Using this special type brazing flux, 5A02 aluminium sheet could be joined to Q235 steel sheet by large spot Nd∶YAG laser-pulsed MIG hybrid welding. Weld appearance and mechanical properties and component of the joints as well as the function of each composition of the brazing flux were analyzed. The results indicated that a good fusion-brazing weld could be obtained by using $KAlF_4$+Sn+Zn brazing flux on the Q235 steel sheet, and the process was stable. The tensile strength of the joint could reach 167. 3 MPa, about 83. 6% of the aluminium base metal, which is equivalent to the fusion joint by conventional arc welding. The fracture of the joints was within the heat-affected zone on the aluminium side, and the heat-affected zone is intenerated appreciably. The fracture morphology mainly was ductile with somewhat brittle. The shear strength of the joint was up to 106. 3 MPa. The SEM test results showed that an intermetallic compounds layer was found in the joint, but the thickness of the layer was only about 3. 27 μm. The EDS test results showed that around the brazing interface Al and Fe atoms diffused sufficiently with each other.

Key words: laser; pulsed MIG arc; hybrid welding; fusion-brazing joining; special flux

Effect of surface nanocrystallization of MCrAlY coating on TGO WANG Zhiping[1], PANG Ying[2], FENG Ribao[1], DING Kunying[1] (1. College of Sciences, Civil Aviation University of China, Tianjin 300300, China; 2. College of Safety, Civil Aviation University of China, Tianjin 300300, China). p25—28

Abstract: Thermal barrier coating, obtained by high velocity oxygen fuel thermal spraying (HOVF) on GH99 high-temperature alloy was treated by supersonic fine particles bombarding, and its influence on microstructure and thermally grown oxide (TGO) of MCrAlY bond coating was studied. The experimental results show that the diffusision access of Al-element increased with supersonic treating, then Al_2O_3 formed quickly on MCrAlY surface, and Ni, Cr were prevented from oxidizing. For this reason, $Ni(Cr, Al)_2O_4$, NiO avoided forming, and flaw decreased, so that the high temperature oxidation resistance of coating con be improved.

Key words: thermal barrier coating; supersonic fine particles bombarding; thermally grown oxide

Anti-fatigue optimization design of welded structure DING Yanchuang, ZHAO Wenzhong (School of Mechanical Engineering, Dalian Jiaotong University, Dalian 116028, Liaoning, China). p29—32

Abstract: Optimization design method of welded structure was put forward with welded joint fatigue damage as constraints. According to International Institute of Welding (IIW) standards and Miner cumulative damage theory, virtual fatigue test (VFT) was presented to predict the welded joint' s fatigue accumulation damage. Approximation models based on design of experiments (DOE) were used to improve optimization efficiency. The anti-fatigue lightweight design of welded bogie frame was preformed using this method. According to UIC515—4, the maximum extraordinary stress and the three key welded joints fatigue damage are considered as constraints, the plate thickness as design variables and the minimum mass as the object function. Latin Hypercube method was used with 10 design variables to provide 120 sample points, and approximation models for bogie frame' s strength and fatigue analysis are constructed using Kriging model. The optimization with sequential quadratic programming algorithm is performed on Kriging approximate model, and mass reduced by 11. 6%. This method has some reference value to the anti-fatigue design of complex welded structure.

Key words: welded structure; fatigue damage; optimization design; virtual fatigue test; approximation model

On-line detection of underwater molten pool width based on structured light ZHANG Weimin[1,2], WANG Guorong[1], SHI Yonghua[1], LI Hexi[1] (1. School of Mechanical Engineering, South China University of Technology, Guangzhou 510640, China; 2. Department of Computer Science and Information Technology, Guangzhou Maritime College, Guangzhou 510725, China). p33—36

Abstract: It is very difficult to detect molten pool width by directly acquiring its in underwater welding. Based on strip-structured weld image, a on-line detection method of molten pool width is proposed. The laser-structured vision sensor is fixed behind the welding torch and put into water with waterproof guard. According to the feature of underwater weld image, the molten pool width is extracted through window processing, laplace sharpening, thresholding, mathematic morphology filtering and thinning procedure. The experimental results show that the processing speed is fast and the detection precision is high. If the distance between the molten pool centre and the strip light detecting point is less than 35 mm, the comparative error of molten pool width can be controlled within 3%.

Key words: underwater welding; molten pool width; strip-structured light; image processing

Simulation on temperature field for Invar alloy during TIG welding XU Peiquan[1], ZHAO Xiaohui[2], HE Jianping[1], XU Guoxiang[1], YU Zhishui[1] (1. College of Materials Engineering, Shanghai University of Engineering Science, Shanghai 201620, China; 2. Institute of Welding Technology, DHI·DCW Group Co., Ltd., Dalian 116031, Liaoning, China). p37—40

Abstract: According to TIG welding character of Invar alloy and 45 carbon steel, geometric model was founded and double ellipsoid heat source model was selected as welding heat source. Temperature fields of base materials with different thickness were simulated using ANSYS, and coupled field of temperature and stress was realized to simulate the residual stress distribution. Experiments under different thickness and welding parameters were carried out and distortion of base materials with different position was detected. Thus comparison between simulation results and experimental results can be carried out. The results show, welded joint with well metallurgy and penetration of invar alloys can be obtained using welding parameters of 132 A, 17.1 V, 4 mm/s and 1.88 mm thickness; and the results of temperature fields simulated by finite element method accords well with experiment results.

Key words: Invar alloy; TIG welding; temperature field

Comparison of two modeling method of 3D curve welding seam CHEN Haiyong[1], XU De[1], WANG Hong[2] (1. Institute of Automation, CAS, Beijing 100080, China; 2. Control Systems Centre, School of Electrical and Electronics Engineering, the University of Manchester, Manchester M601QD, UK). p41—44

Abstract: Three Dimension (3D) curve welding seam modeling is one of key technologies for seam tracking. The model can reduce the noise interference, improve the stability and robustness of welding system. Moreover, the system can obtain the fault tolerant ability from the model. The 3D curve welding seam was represented by using cubic parametric curve function, then the cubic parametric curve seam position model was obtained by using least square (LQ). Furthermore, the position model was also established by using cubic B spline approximation. The pose model was gotten by employing the position model and other welding seam coordinates. The performance of the two model was compared and analyzed. Simulation result verifies that B spline seam model excel the cubic parametric curve seam model and provid better approximation to the original welding seam.

Key words: 3D welding seam model; B spline function; cubic parametric curve function

Quality of resistance spot welding based on variable electrode force SUN Haitao, ZHANG Yansong, LAI Xinmin, CHEN Guanlong (School of Mechanical Engineering, Shanghai Jiaotong University, Shanghai 200240, China). p45—48

Abstract: Hot dipped galvanized (HDG) low carbon steels have been widely used in internal and outside plates of auto body. Constant electrode force was utilized under conventional pneumatic guns, which led to unstable welding quality. However, the quality of resistance spot welding (RSW) on galvanized steels was sensitive to variable electrode force. Considering controlling electrode force exactly with servo guns, a design of experiment (DOE) method was applied to analyze the influence of three stages of electrode force during the welding process, including preliminary force, welding force and forging force, on welding quality and to obtain optimum parameters of variable electrode force. The results showed that forging force was noted as the most important factor, welding force as secondary one, squeeze force as least important one, and that optimum parameters could increase tensile-shear force and nugget diameter of welds significantly. This method would be the foundation of real-time quality evaluation and control based on electrode force.

Key words: electrode force; DOE method; hot dipped galvanized low carbon steels; resistance spot welding

Welding characteristics of Al/Ti dissimilar alloys by laser welding-brazing with different spot CHEN Shuhai, LI Liqun, CHEN Yanbin (State Key Laboratory of Advance Welding Production Technology, Harbin Institute of Technology, Harbin 150001, China). p49—52

Abstract: Ellipse spot and rectangular laser spot were used as the heat source respectively to experimentally research laser welding-brazing with filler wire for Al/Ti dissimilar alloys. And the influence of gap and heat input on weld appearance were analyzed, furthermore, the welding interface characteristics with different heat source were obtained. Experimental results show that both ellipse spot and rectangular beam can gain the good weld appearance. Increasing heat input is of advantage to enhance the interface strength, but it is of disadvantage to control the weld appearance. Welding stability and processing control with rectangular spot are better than those with ellipse spot. The maximum tensile strength of joint gained by ellipse spot and rectangular spot is respectively high up to 75% and 80% of aluminum base material.

Key words: rectangular spot; ellipse spot; laser welding-brazing; Al/Ti dissimilar alloys

Kinetic analysis of spray transfer welding arc in a longitudinal magnetic field HUA Aibing, CHEN Shujun, ZHANG Xiaoliang, YIN Shuyan (College of Mechanical Engineering and Applied Electronics Technology, Beijing University of Technology, Beijing, 100124, China). p53—56

Abstract: A miniaturized generator device for longitudinal